

**The Effect of Restricted Ankle Dorsiflexion on Knee Injury Risk
During Landing**

Zanni Zhang¹, Datao Xu^{1,2}, Meizi Wang^{1,3}, Huiyu Zhou¹, Minjun Liang¹, Julien S.
Baker¹, Yaodong Gu^{1*}

¹Faculty of Sport Science, Ningbo University, Ningbo, China

²Faculty of Engineering, University of Pannonia, Veszprem, Hungary

³Department of Biomedical Engineering, Faculty of Engineering, Hong Kong Polytechnic University,
Hong Kong SAR, China

*Corresponding author: Yaodong Gu, Faculty of Sport Science, Ningbo University, Ningbo, China,

e-mail address: guyaodong@nbu.edu.cn

Submitted: 11th December 2024

Accepted: 19th February 2025

29 **Abstract:**

30 **Purpose:** This study utilized a combination of musculoskeletal modeling and finite
31 element analysis to investigate the effects of varying ankle dorsiflexion ranges on knee
32 joint loading, soft tissue stress distribution, and the coactivation patterns of muscles
33 surrounding the knee during landing.

34 **Methods:** Based on the Weight-Bearing Lunge Test (WBLT), a total of 32 basketball
35 players into two groups: normal dorsiflexion (ND) and limited dorsiflexion (LD) and
36 conducted six countermovement jumps (CMJ) while collecting motion and force data.
37 Personalized musculoskeletal models were created using OpenSim to analyze
38 kinematics and kinetics, and Helium-free MRI and CT scans were used for finite
39 element modeling to assess internal tissue stress in the knee.

40 **Results:** During landing, the patellofemoral joint contact force in LD was reduced
41 compared to the ND. The coactivation of muscles around the knee joint decreased. The
42 von Mises stress in the tibial cartilage, meniscus, anterior cruciate ligament, and
43 posterior cruciate ligament were elevated.

44 **Conclusions:** The results suggest that increased ankle dorsiflexion during landing may
45 effectively reduce internal tissue stress in the knee joint while enhancing muscle
46 coactivation around the knee joint and increasing patellofemoral joint contact force.
47 These findings provide valuable theoretical support for strategies to reduce the risk of
48 knee injuries during landing. Additionally, they offer reliable technical approaches and
49 theoretical insights for studying injury mechanisms in other sports activities, such as
50 running and lateral jumping.

51
52 **Keywords:** Ankle dorsiflexion, Landing injury, Finite element analysis, Helium-free
53 MRI, Opensim, Musculoskeletal modeling

54

55 **1. Introduction**

56 During the performance of high-intensity sports, especially basketball, where
57 activities such as jumping and rapid movements are integral, injuries to the lower limbs

58 are among the most prevalent types of injury sustained by athletes [33], the cause of
59 this damage is largely due to excessive impact force [16]. The ankle joint, as the first
60 movable joint in contact with the ground, is one of the key anatomical structures that
61 reduces the impact force on the lower limbs in jumping sports. Ankle motion plays a
62 crucial role in sports performance and injury risk [76], especially during jumping and
63 landing. Ankle function directly affects the knee and hip joints' movement pattern and
64 load distribution.

65 The dorsiflexion ability of the ankle joint not only impacts on an athlete's ability
66 to jump but is also closely linked to stability during landing. During jumping
67 movements, the landing phase imposes significant demands on joint impact forces and
68 muscle coordination. Insufficient ankle function can increase energy demands on the
69 proximal joints [35, 72]. During landing, the knee joint, which serves as a critical link
70 between the ankle and hip, is highly vulnerable to injury [24, 74]. Existing studies
71 suggest that increasing the angle of ankle plantarflexion during landing may reduce the
72 impact forces transmitted to the knee joint, thereby decreasing the risk of injury to the
73 medial femoral attachment of the anterior cruciate ligament (ACL) [64]. Additionally,
74 reduced ankle mobility in basketball players has been shown to contribute to patellar
75 joint pain [1, 61]. Healthy female athletes typically exhibit a larger dynamic range of
76 motion (ROM) during takeoff and landing. Conversely, limited ankle dorsiflexion is
77 linked to a higher risk of injury during jump landing activities. Adjusting the initial
78 ankle contact angle has been suggested as a potential strategy to reduce knee joint injury
79 risk [49]. Repeated exposure to high-impact forces on the knee can result in non-contact
80 ACL injuries, meniscal damage, and cartilage injuries.

81 Amongst the many jumping tests used in medical and performance evaluation, the
82 Countermovement Jump (CMJ) test, widely used to assess explosive power and lower
83 limb biomechanics, has become a standard tool in sports medicine and biomechanical
84 research [52]. The CMJ test effectively simulates jumping and landing movements
85 typically seen in sports scenarios [48]. Previous studies have compared the effects of
86 squat jumps and CMJ at different starting positions on athletic performance, revealing
87 that CMJ utilizes rebound force more efficiently, resulting in higher jump heights [21].

88 Power output and explosive force can be optimized by adjusting the starting position
89 and movement speed, thereby enhancing jump performance [45]. While various factors
90 influencing CMJ landing have been explored, the impact of ankle dorsiflexion ROM
91 on lower limb biomechanics during CMJ has not received adequate attention.

92 In recent years, musculoskeletal modeling and finite element analysis (FEA), have
93 evolved as important tools in lower limb motion biomechanics research, and have been
94 widely used in sports injury prediction, sports performance optimization and
95 rehabilitation [11, 13]. FEA and OpenSim are both vital tools used in the study of lower
96 limb biomechanics. FEA divides the lower limb's bone, muscle, and joint structures
97 into multiple small elements through numerical simulations, enabling accurate analysis
98 of stress distribution during movement. This helps in evaluating sports injuries,
99 optimizing athletic posture, and designing artificial joints. FEA is widely used in sports
100 injury prediction, rehabilitation, and prosthesis design [24, 71, 73]. Previous studies
101 employing FEA have examined factors such as joint stress distribution at different
102 contact angles during running, as well as stress response patterns in individuals with
103 lateral ankle ligament injuries [71, 77, 80]. Previous studies have employed recumbent
104 Magnetic Resonance Imaging (MRI) for joint imaging and structural analysis of
105 subjects [5, 8]. While recumbent MRI is typically used for static structural analysis, its
106 inability to fully simulate dynamic motion has limited the comprehensive study of
107 dynamic processes. In contrast, multi-position Helium-free Magnetic Resonance
108 Imaging (MRI) technology allows for joint scanning in an upright position, enabling
109 the capture of the position and shape of soft tissues such as joints and ligaments under
110 the subject's own weight [2]. Moreover, Helium-free MRI utilizes a superconducting
111 magnet system that does not rely on liquid helium cooling, significantly reducing both
112 equipment costs and maintenance complexity, while offering enhanced image
113 resolution and shorter scan times. OpenSim is a simulation tool that models the
114 interactions between muscles, bones, and joints, facilitating the analysis of mechanical
115 changes across different movement patterns. It plays a pivotal role, particularly in gait
116 analysis, musculoskeletal dynamics, and rehabilitation training [56, 75]. Some studies
117 have used the OpenSim model to simulate the effect of limited ankle dorsiflexion

118 motion on starting and stopping movements, and the results demonstrate that knee
119 stability is enhanced when the ankle dorsiflexion angle is restricted [75]. However,
120 there is a lack of systematic research on the impact of ankle dorsiflexion motion during
121 the CMJ process, particularly regarding its influence on knee injury risk.

122 This study aims to combine musculoskeletal modeling and finite element analysis
123 of the lower extremities to simulate the effects of varying ankle dorsiflexion movements
124 on the biomechanical characteristics during the CMJ landing. The goal was to clarify
125 the specific manifestations and patterns of knee injury risk under different ankle
126 dorsiflexion conditions. The study hypothesizes that during the landing phase, a
127 reduced ankle dorsiflexion ROM will lead to increased knee joint stress and a higher
128 risk of injury, with the knee joint exhibiting adaptive changes to compensate for the
129 restricted dorsiflexion range.

130

131 **2. Methods Details**

132 *2.1 Study Participant Details*

133 The sample size for this study was calculated using G*Power software (version
134 3.1.9.7; Heinrich Heine University Düsseldorf, Düsseldorf, Germany), based on effect
135 sizes reported in previous studies examining biomechanical differences in lower limb
136 movements between individuals with and without ankle dorsiflexion limitations. The
137 analysis aimed to ensure sufficient statistical power (≥ 0.8) to detect significant
138 differences in joint angle, torque, and muscle activation patterns during the CMJ
139 landing, with the alpha level set at 0.05. Power analysis indicated that a minimum
140 sample size of 25 participants would be adequate [55]. To account for potential dropouts
141 and to enhance the robustness of the analyses, 32 male basketball players were recruited
142 for this trial. Inclusion criteria were as follows: (1) participants aged 18-30 years; (2)
143 regular engagement in basketball training, characterized by a minimum of three
144 sessions per week, each lasting at least two hours; (3) no history of lower limb surgery
145 or significant musculoskeletal injury in the past 6 months; (4) no underlying
146 neurological or systemic conditions that might affect motor function.

147 To assess whether participants had limited ankle dorsiflexion, the Weight-Bearing

148 Lunge Test (WBLT) was employed [25, 54]. The WBLT is a reliable and commonly
149 used clinical assessment for evaluating ankle dorsiflexion ROM in a functional, weight-
150 bearing position. During the test, participants were instructed to keep their heel
151 grounded and their feet flat on the floor, performing a lunge by advancing the knee
152 towards a wall while maintaining heel contact with the ground. The participant was then
153 asked to slowly bend the front knee and lunge forward as far as possible, aiming to
154 bring the knee as close to or in contact with the wall without lifting the heel. Ankle
155 flexibility was assessed by measuring the dorsiflexion angle using a protractor. The test
156 was terminated if the heel was raised off the ground. The maximum dorsiflexion angle
157 achieved while maintaining heel contact with the ground was recorded to accurately
158 reflect the ankle joint's ROM. Three trials were conducted, and the average value was
159 used for analysis.

160 Following the WBLT screening, participants were divided into two groups: the
161 normal dorsiflexion (ND) group (n = 17, height: 184.6 ± 3.5 cm; age: 21.3 ± 1.5 years;
162 weight: 75.4 ± 2.6 kg) and the limited dorsiflexion (LD) group (n = 15, height: $183.2 \pm$
163 2.8 cm; age: 22.1 ± 1.8 years; weight: 76.4 ± 3.1 kg). The use of the WBLT provided a
164 functional assessment of ankle mobility, ensuring that the classification accurately
165 reflected participants' ability to dorsiflex during weight-bearing activities. The
166 comparison of average dorsiflexion amplitude of ankle joint between the normal
167 dorsiflexion group and the limited dorsiflexion group is shown in Table 1 Prior to data
168 collection, all participants were thoroughly briefed on the study's objectives, procedures,
169 conditions, and requirements. This ensured a more precise investigation of how
170 limitations in dorsiflexion could influence lower limb biomechanics during dynamic
171 movements, such as CMJ landing. Comprehensive details regarding the study were
172 outlined in the consent form, and the study protocol was approved by the Ethics
173 Committee of Ningbo University (Protocol code: TY2024031).

174 **Table 1:** Comparison of mean ankle dorsiflexion range between normal dorsiflexion
175 group and limited dorsiflexion group.

	ND (n = 17)	LD (n = 15)	P
--	-------------	-------------	---

	Mean ± SD	Mean ± SD	
Ankle dorsiflexion range in dominant leg (°)	40.2 ± 3.1	34.1 ± 2.9	0.032*
Ankle dorsiflexion range in the nondominant leg (°)	39.5 ± 2.4	34.3 ± 2.7	0.044*

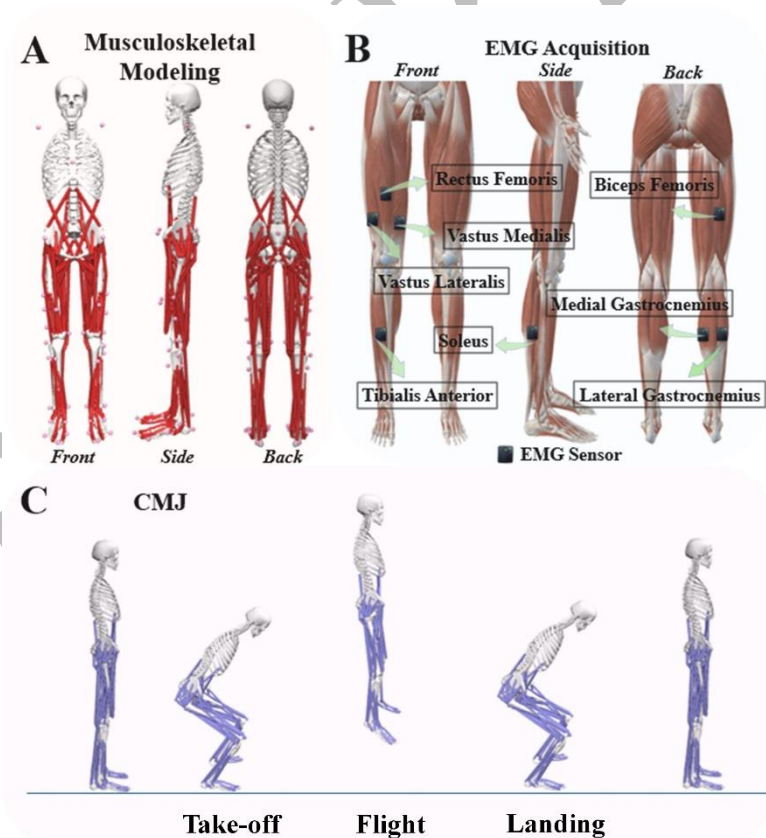
176 Note: "*" indicates a significant difference in ankle dorsiflexion ROM between the two groups ($p < 0.05$).

177 2.2 Biomechanics parameters collection and processing

178 In this study, participants were instructed to wear exercise tights and were fitted
179 with reflective markers according to the Gait2392 musculoskeletal model, which
180 features 23 joint degrees of freedom and 92 muscle-tendon actuators within the
181 OpenSim framework (Figure 1A). Electromyographic (EMG) signals were recorded
182 from the target muscles using an EMG testing system (Figure 1B). Motion trajectories
183 were captured using the Vicon 3D motion capture system (Vicon Metrics Ltd., Oxford,
184 UK), while ground reaction forces were measured with an AMTI force platform (AMTI,
185 Watertown, MA, USA). Kinematic and kinetic data were acquired at sampling
186 frequencies of 200 Hz and 1000 Hz, respectively [65, 66]. EMG signals were recorded
187 at 1000 Hz using the Delsys EMG system (Delsys, Boston, Massachusetts, USA) [66].
188 Before the start of the formal experiment, the calibration of the experimental equipment
189 should be carried out first, and the stray points outside the experimental environment
190 should be deleted in the Vicon system to avoid affecting the experimental environment.
191 Then, the calibration rod with reflective marks should be held around the force table to
192 ensure the normal operation of the camera and the normal acquisition of all reflection
193 points. After that, the calibration rod is placed on the corner of the force measuring table
194 to establish a spatial coordinate system. After the coordinate system is established, it is
195 determined whether there is a hybrid force on the force measuring table. If there is a
196 hybrid force, it needs to be eliminated manually. After the environmental calibration of
197 the experimental equipment, static and dynamic test collection is carried out.

198 To ensure optimal performance and minimize the risk of injury, participants
199 completed a 10-minute warm-up (including jogging, jumping, and stretching) at an

200 adaptive intensity before the test. During the CMJ test (Figure 1C), participants started
201 hip-width apart and slightly rotated to provide stable support. They then crouched to
202 stretch the lower limb muscle groups and connective tissues, with the arms positioned
203 behind the body in preparation for the swing. Subsequently, participants swung their
204 arms forward vigorously, extended their hips, and jumped upwards as quickly as
205 possible, maintaining a straight posture to achieve maximum height [43]. Upon landing,
206 the front foot contacted the ground first, followed by the heel, and participants returned
207 to a standing position. The study conducted a repeat test for each participant, in which
208 each participant performed six jumps with a one-minute rest period between each jump,
209 to prevent fatigue-related injuries and ensure the accuracy of the experimental data.
210 Participants were instructed to exert 100 percent effort during each takeoff and to
211 stabilize their bodies as much as possible during the landing. A sliding or unstable
212 landing is recorded as a failure [78].

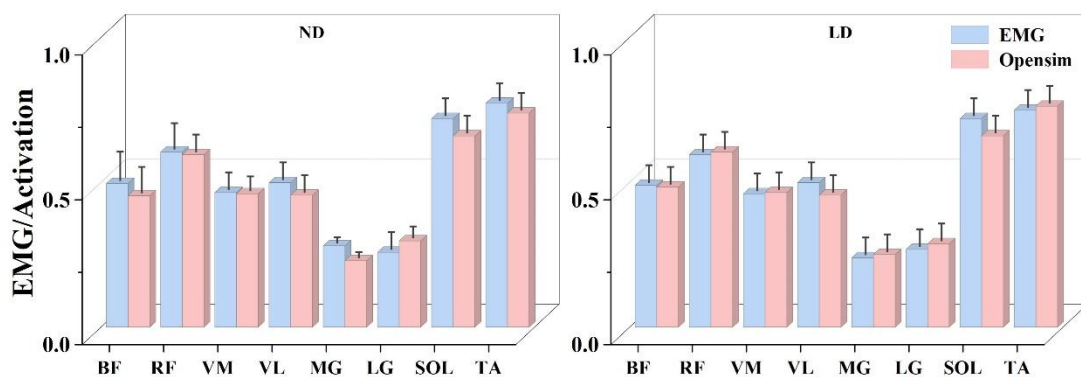


213

214 **Figure 1:** (A) Schematic representation of marker points in the Opensim
215 musculoskeletal model. (B) Schematic representation of EMG test locations. (C)
216 Schematic representation of CMJ test.

217

218 The landing phase was defined as the period from initial contact, when the ground
219 reaction force exceeded 10 N, to maximum knee flexion [47]. Data on motion
220 trajectories and ground reaction forces, simultaneously recorded by the Vicon motion
221 capture system and AMTI force platform, were imported into MATLAB (Matlab
222 R2022a, MASS, Natick, MA, USA) for analysis. The kinematic and kinetic data,
223 originally in (.c3d) format, were transformed into (.trc) and (.mot) formats for further
224 analysis in OpenSim. To enhance the accuracy of the model, the marker weights were
225 adjusted based on the subjects' anthropometric parameters, ensuring that the subject-
226 specific model aligned with the 2392 model when both were loaded. Joint angles were
227 computed using inverse kinematics, while joint moments were determined through
228 inverse kinetics [31]. Static optimization algorithm was employed to estimate muscle
229 activation and muscle forces. The raw EMG signals were first filtered using a fourth-
230 order Butterworth bandpass filter (10–500 Hz) in the Delsys EMG analysis software,
231 after which the root mean square (RMS) values were calculated. To normalize the EMG
232 amplitudes, they were expressed as a percentage of the maximal voluntary isometric
233 contraction (MVIC) for each muscle. Muscle activation levels were quantified on a
234 scale from 0 (no activation) to 1 (full activation) by dividing the RMS amplitude during
235 the test by the RMS amplitude from the MVIC. The muscle activation data obtained
236 from the EMG sensors were compared with the musculoskeletal model simulation
237 results to evaluate the model's accuracy and validity. No significant differences were
238 found between the activation levels from the EMG data and those from the
239 musculoskeletal model simulations (Figure 2).



240

241 **Figure 2:** Schematic representation of EMG muscle activation with blue areas
 242 representing EMG muscle activation results and red areas representing muscle
 243 activation results from the musculoskeletal model. The vertical scale ranges from 0 to
 244 1, indicating the level of muscle activation from none to full activation.

245

246 The coactivation of muscles surrounding the knee joint during the landing phase
 247 of the CMJ was determined using the following formula[44]:

$$248 \quad \text{Muscleco - activation}(\%) = \left(\frac{RMSEMG_{antagonist}}{RMSEMG_{agonist}} \right) \times 100 . \quad (1)$$

249 During the CMJ landing phase, the patellofemoral joint contact force (PTF) is
 250 determined using the following formula:

251 (x) represents the knee flexion angle, (Mk) represents the knee extensor moment [28].

252 The knee flexion angle was determined using the nonlinear equation for the quadriceps
 253 lever arm, as described below [34]:

$$254 \quad Lq = 0.00008x^3 - 0.013x^2 + 0.28x + 0.046 . \quad (2)$$

255 The strength of the quadriceps (Fq) refers to quadriceps strength:

$$256 \quad Fq = \frac{Mk}{Lq} . \quad (3)$$

257 The constant k is the constant that correlates with the knee angle position [60]:

$$258 \quad K = \frac{0.462 + 0.00147x^2 - 0.0000384x^2}{(1 - 0.0162x^2 + 0.000155x^2 - 0.000000698x^3)} . \quad (4)$$

259 The PTF was calculated based on the quadriceps force (Fq) and a constant k :

$$260 \quad PTF = Fq \times k . \quad (5)$$

261 2.3 Quantification and Statistical Analysis

262 This study examined changes in lower limb biomechanics during the landing phase
 263 of the CMJ. The biomechanical data were normalized to 101 data points, representing
 264 the full range from 0% to 100% of the landing phase. All variables in this study are
 265 normally distributed after Shapiro-Wilk test. To assess differences in joint kinematics
 266 and kinetics between the two groups, independent sample t-tests were conducted, with
 267 statistical analysis performed using SPSS 27. The significance level was set at $p < 0.05$.
 268 Lastly, the data were imported into Origin 2022 software for graphical representation

269 and visualization.

270

271 **3. Finite element analysis of foot-knee integration model**

272 *3.1 Model construction*

273 Two healthy male subjects, with no history of ankle and knee pain or lower
274 extremity surgery, underwent magnetic resonance imaging (Helium-free MRI) and
275 computed tomography (CT) scans to assess those with high and low ankle dorsiflexion
276 ROM, respectively. While standing, the knee joint was fully extended, and the ankle
277 joint was positioned in a neutral alignment. The knee joint was subsequently scanned
278 using a Helium-free MRI system (Figure 3A). The repetition time and echo time were
279 set to 500 ms and 14 ms, respectively, with a 20 cm field of view and a slice thickness
280 of 1 mm. During the MRI image processing and model creation, the images were
281 imported into Mimics 21.0 (Materialise, Leuven, Belgium), where bone and soft tissue
282 boundaries were identified and segmented using gray value determination and region-
283 based segmentation techniques. These were then exported in STL file format. The bone,
284 ligaments, and skin were imported into Geomagic Studio 2021 (Geomagic, Inc.,
285 Research Triangle Park, NC, USA) for noise reduction, smoothing, surface creation,
286 and fitting, and subsequently exported in IGES format. Each component was converted
287 into a solid using SolidWorks 2022 (SolidWorks Corporation, Waltham, MA, USA),
288 and the joint position was assembled based on orthogonal plane projections of the
289 subject's knee joint during landing, ensuring consistency with the actual X-ray images.
290 The model was subsequently constructed in Workbench 2021 (ANSYS, Inc.,
291 Canonsburg, PA, USA), where contact conditions were specified, and the tetrahedral
292 mesh was employed for model discretization (Figure 3B). After performing a mesh
293 convergence test, the bone mesh was set to a size of 2.0 mm, while the mesh size for
294 the anterior cruciate ligament (ACL) and posterior cruciate ligament (PCL) was reduced
295 to 0.5 mm. The meniscus, ligaments, and cartilage were assigned to a mesh size of
296 1.0mm.

297 *3.2 Material properties, boundaries, and loading conditions*

298 All materials, except for the encapsulated soft tissue, ACL, and PCL, were

299 modeled as linear elastic, with their elasticity characterized by Young's modulus (E) and
 300 Poisson's ratio (ν). The soft tissue, ACL, and PCL were treated as hyperelastic materials,
 301 represented using the Mooney-Rivlin model. The material properties for each
 302 component are provided in Table 2.

303 **Table 2:** Material parameters for each structure.

Component	Elastic modulus (MPa): E	Poisson's ratio: ν	Density (kg/m ³)	Ref
Skin	Hyperelastic (first-order Ogden model, $\mu=0.122\text{kPa}$, $\alpha=18$)	N/A	950	[50]
Bulk soft tissue	Hyperelastic (secondorder polynomial strain, $C_{10}=0.8556$, $C_{01}=0.05841$, $C_{20}=0.03900$, $C_{11}=0.02319$, $C_{02}=0.00851$, $D_1=3.65273$)	N/A	950	[24]
Anterior Crucial Ligament	Hyperelastic (first-order polynomial strain, $C_1=1.95$, $D=0.00683$)	N/A	1000	[51]
Posterior Crucial Ligament	Hyperelastic (first-order polynomial strain, $C_1=3.25$, $D=0.0041$)	N/A	1000	[51]
Fibula, Tibia, Femur, and Patella	14220	0.3	1990	[27]
Foot Bones	7300	0.3	1500	[12]
Knee Cartilages	20	0.46	1000	[38]
Foot Cartilages	1	0.4	1050	[57]
Medial and Lateral	467	0.46	1000	[20]

Collateral				
Ligament				
Medial and				
Lateral	59	0.49	2000	[37]
Meniscus				
Patellar	778	0.46	1000	[3]
Tendon				
Foot	260	0.4	1000	[57]
Ligaments				
Plantar Fascia	350	0.4	1000	[9]
Patellar	816	0.3	1000	[10]
Tendon				
Plate	17000	0.4	1000	[79]

304 Building on this foundation, the model was locally refined according to the
305 geometric features of the contact areas. A contact group was subsequently created to
306 define the bonding relationships between the cartilage and bone, as well as between the
307 origins of each ligament and bone, and the meniscus and bone. To model the sliding
308 friction between the meniscus and femoral cartilage, as well as between the patellar and
309 femoral cartilage, a friction coefficient of 0.04 was applied [23, 26]. Frictionless contact
310 between cartilage and the bone surface and between the ACL and PCL was defined
311 based on previous indications [4]. The anchor points of bone and cartilage are
312 encapsulated soft tissues. For the foot-knee model placement, the knee joint was preset
313 to a neutral position. The knee joint angle was determined by adjusting the angle
314 between the femoral axis, tibial axis, and the longitudinal axis of the foot in the sagittal
315 plane [23]. A fixed ground plate and femoral interface were used for the analysis, with
316 a contact surface featuring a friction coefficient of 0.6 to model the foot-ground
317 interaction, while the femoral interface remained stationary (Figure 3D) [68]. The peak
318 ground reaction force during CMJ landing, along with the corresponding kinematic,
319 kinetic, and muscle force data used for the finite element (FE) analysis, are presented

320 in Table 3.

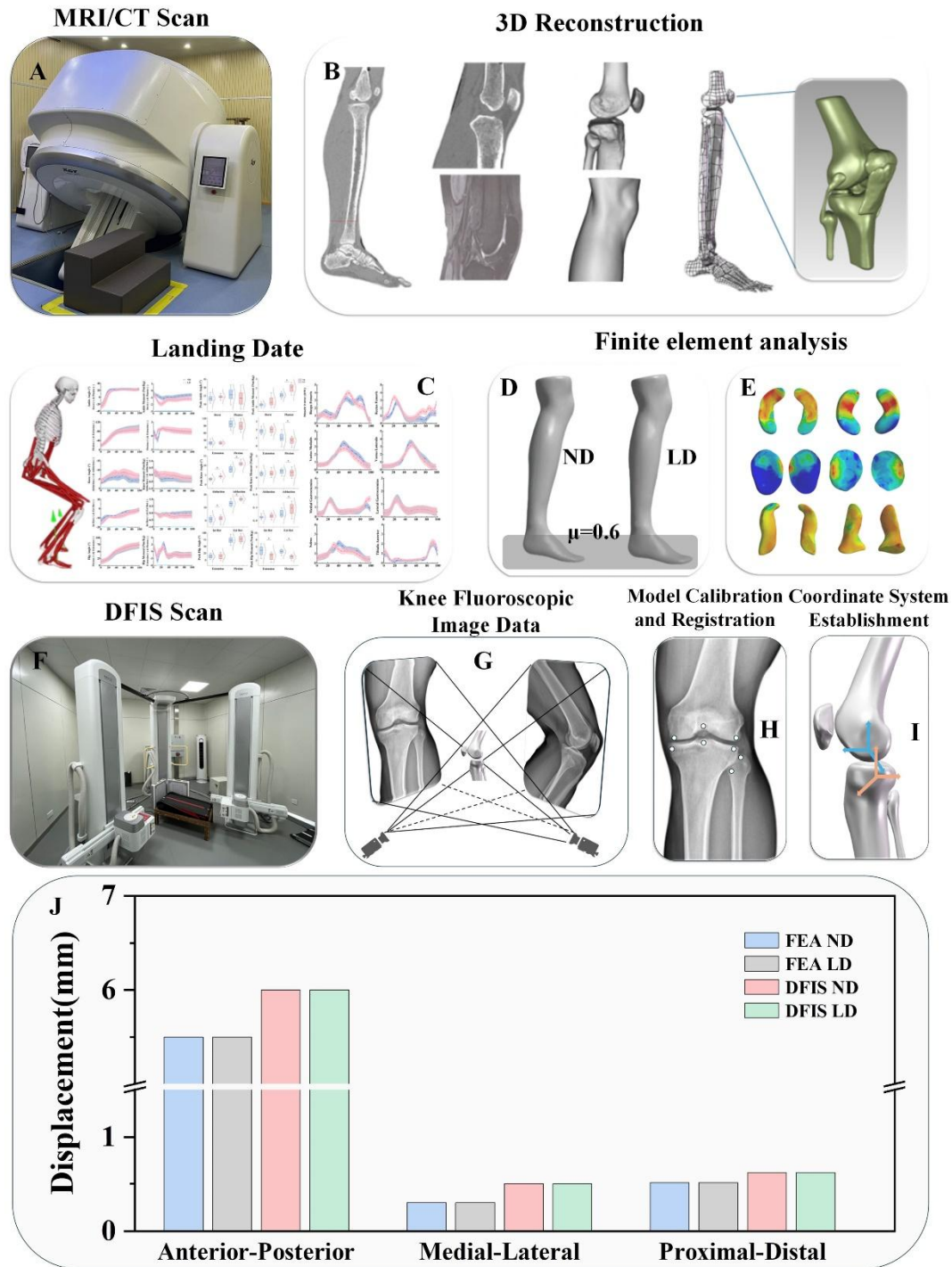
321 **Table 3:** Finite element model of the knee joint with applied loads.

Experimental variables		ND	LD
Ground Reaction Force (N)	Posterior	254.15	251.40
	Medial	231.16	226.34
	Vertical	1562.22	1801.27
Ankle Angle (°)	Dorsiflexion	24.18	26.24
	Flexion	94.35	89.85
Knee Angle (°)	Adduction	1.44	1.31
	Ext Rot	10.10	13.07
	Biceps Femoris	360.77	348.23
Muscle Force (N)	Rectus Femoris	974.89	1116.03
	Vastus Medialis	196.56	150.43
	Vastus Lateralis	356.18	324.48
	Medial Gastrocnemius	499.91	661.37
	Lateral Gastrocnemius	180.69	146.42
	Soleus	378.30	370.70
	Tibialis Anterior	684.71	671.56

322 *3.3 Model validation*

323 In this study, the finite element model was validated through both axial stress and
324 anterior drawer experiments [18, 58, 59]. A 134 N forward thrust was applied to the
325 upper end of the tibia, displacing the midpoint of the tibial intercondylar ridge, like the
326 force used in the anterior drawer test of the knee. Previous studies have reported anterior
327 displacements of 4.0, 4.3, 4.13, and 4.18 mm, which are in good agreement with the
328 simulation result of 4.15 mm obtained in this study, thus confirming the validity of the
329 finite element model [18, 59, 68]. Furthermore, a high-speed double-perspective
330 imaging system (DFIS) (Figure 3F) was employed to capture fluoroscopic images of
331 the subject's knee joint during landing. The DFIS parameters were set as follows: source
332 image distance of 1350 mm, device voltage at 60 kV, device current of 500 mA,

333 exposure time of 3 seconds, laser wavelength of 650 nm, and an automatic exposure
334 control dose range of 45 μ Gy. The flat panel detector had a resolution of 3072×3072
335 pixels, with an X-ray area of 427×427 mm. The X-ray tube operated at a nominal
336 voltage of 150 kV, the laser power was 3 mW, and the angle sector was 90° . The knee
337 joint displacement results obtained from fluoroscopic imaging were compared with the
338 FEA results to further validate the finite element model (FEM) [15, 32, 39]. DFIS
339 captured X-ray information and generated reliable gray-scale medical images after
340 processing the data using different attenuation levels in various tissues and organs
341 (Figure 3F). The Vicon motion capture system and force platform were used to
342 synchronize the kinematic and kinetic data, which were subsequently inputted into the
343 finite element model (Figure 3C). The knee joint image acquired by the fluoroscopy
344 system through two orthogonal planar projections, and the knee joint model was
345 calibrated and aligned using 3D modeling software to ensure consistency with the actual
346 X-ray image (Figure 3G, H). The knee joint displacement accurately calculated using
347 the coordinate system calculator plugin in Rhinoceros software (Figure 8I) [32, 39].
348 The results demonstrate that the knee displacement calculations derived from finite
349 element analysis and DFIS show strong consistency in 3D space, validating the
350 feasibility and reliability of the constructed finite element model (Figure 3J).



351

352 **Figure 3:** Illustration of the finite element model establishment and validation process.

353 (A) Foot and knee data were obtained using CT and MRI scanning techniques. (B)

354 Creation of a finite element model of the knee joint, including the configuration of

355 muscles, bones, and ligaments. (C-E) Import biomechanical data into the finite element

356 model for simulation and visualization of the results. (F-G) Data acquisition and

357 processing of knee joint fluoroscopy images acquired by DFIS. Establishment and

358 registration of (H-I) coordinate system. (J) Comparison of knee displacement calculated
359 based on DFIS and finite element analysis.

360

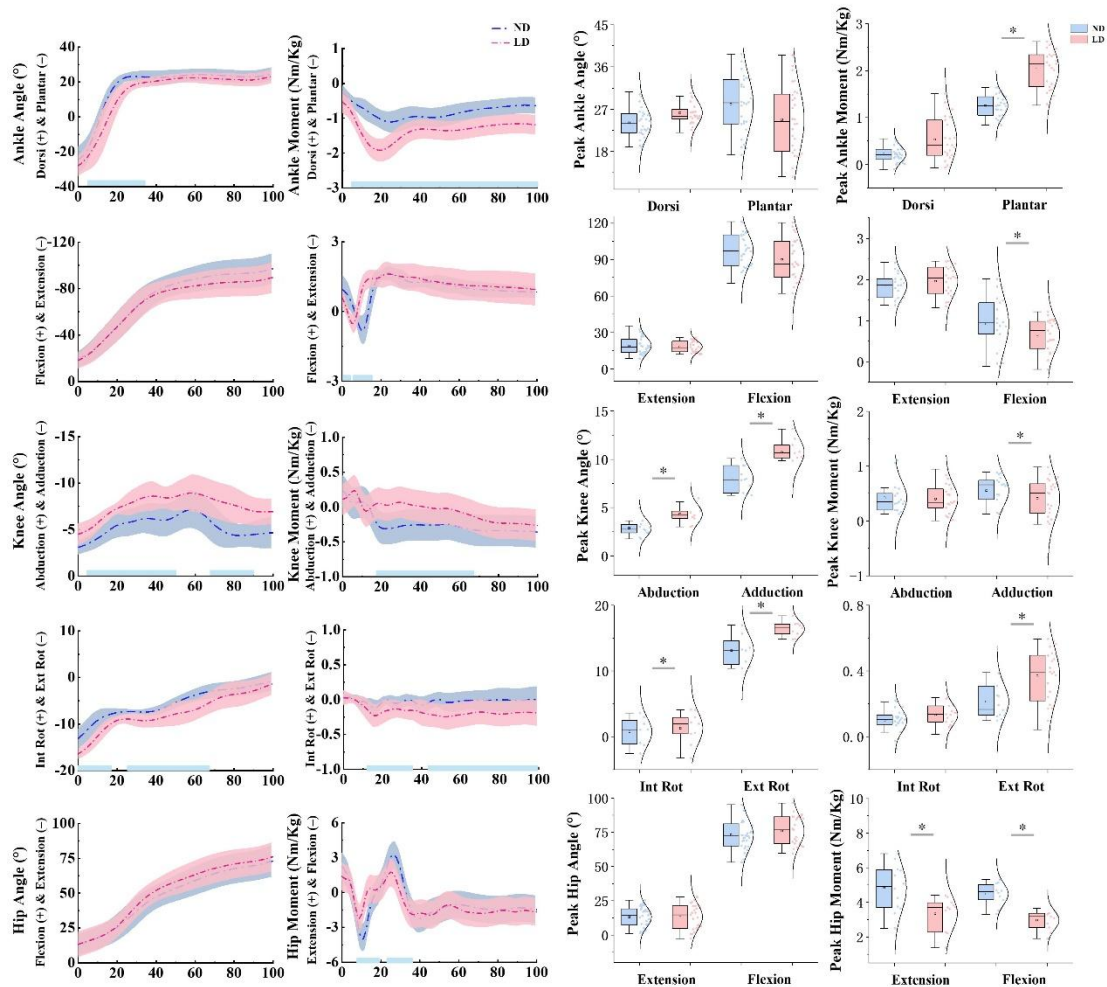
361 **4. Results**

362 *4.1 Kinematics and Kinetics*

363 As shown in Figure 4, the differences in kinematics and kinetics and the peak
364 kinematics and kinetics between ND and LD during the landing phase of the CMJ. In
365 terms of ankle differences, the dorsiflexion Angle of ND was higher than that of LD
366 during the 4%-38% stage ($p < 0.001$), and the ankle moment was higher than that of
367 LD during the whole stage of landing ($p=0.001$). In terms of peak results, the peak
368 plantar flexion moment of the ankle joint was lower in ND than in LD ($p < 0.001$).

369 In terms of knee joint differences, the knee extension moment of ND was greater
370 than that of LD at the 0%-7% stage ($p=0.032$) and was smaller than that of LD at the
371 8%-20% stage ($p=0.021$). The knee abduction Angle was smaller than that of LD at the
372 5%-50% stage and 70%-90% stage ($p=0.003$, $p=0.001$, respectively). The knee
373 abduction moment was lower than LD at 19%-70% stage ($p < 0.001$), and the knee
374 external rotation Angle was lower than LD at 0%-18% stage and 24%-67% stage
375 ($p=0.009$, $p < 0.001$, respectively). The knee external rotation torque was less than LD
376 at 10%-18% stage and 43%-100% stage ($p=0.043$, $p=0.001$, respectively). In terms of
377 peak results, ND had higher knee flexion moments ($p=0.02$), lower abduction and
378 adduction angles ($p=0.04$, $p=0.005$, respectively), higher adduction moments ($p=0.026$),
379 and lower external rotation and internal rotation angles than LD ($p=0.038$, $p=0.005$,
380 respectively). The external rotation torque was less than LD ($p=0.02$).

381 In terms of the difference in the hip joint, ND had a higher hip flexion moment
382 than LD in the 7%-17% stage ($p=0.006$) and lower than LD in the 21%-37% stage
383 ($p=0.01$). In terms of peak results, ND had higher hip extension moment and flexion
384 moment than LD ($p=0.006$, $p < 0.001$, respectively).



385

386 **Figure 4:** Illustration of the kinematic and kinetic differences between ND and LD
 387 during CMJ testing. Blue lines and "*" indicate significant differences ($p < 0.05$).

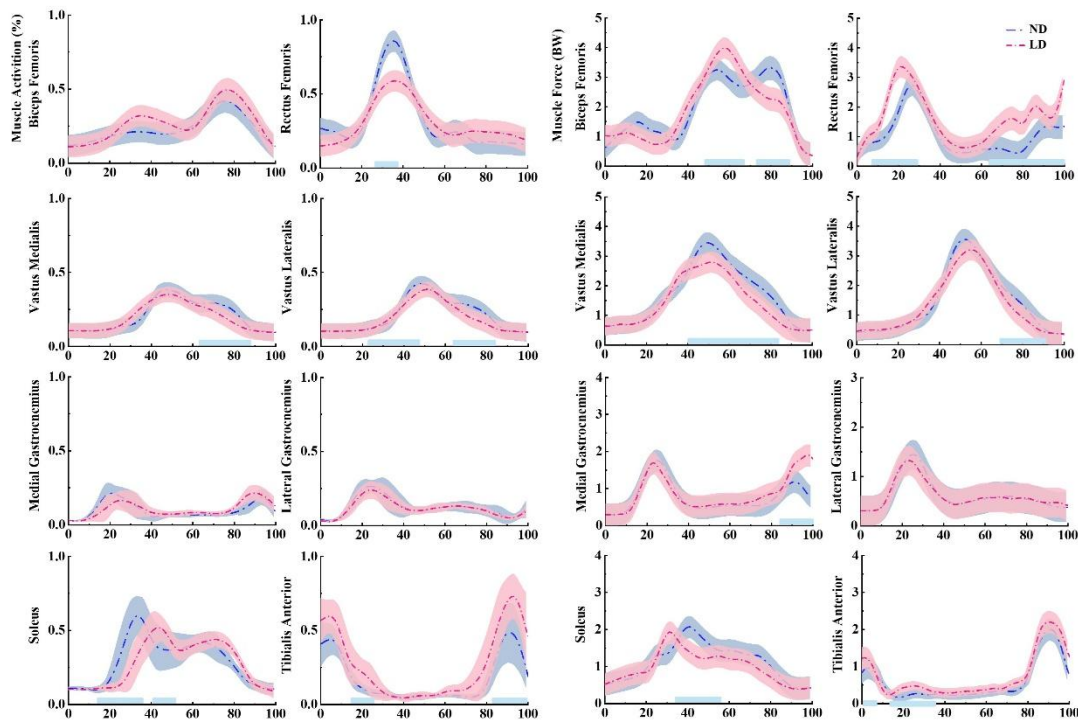
388

389 4.2 Muscle activation and Muscle force

390 As shown in Figure 5, the differences in muscle activation and muscle force
 391 between ND and LD during the landing phase of the CMJ. In terms of muscle activation,
 392 the rectus femoris activation degree of ND was higher than that of LD at 21%-46%
 393 stage ($p < 0.001$) and was lower than that of LD at 72%-91% stage ($p=0.001$). The
 394 vastus medialis activation degree was higher than that of LD at 63%-83% stage
 395 ($p=0.001$). The activation degree of the vastus lateralis muscle was higher than that of
 396 LD at stage 63%-87% ($p=0.001$), and the activation degree of soleus muscle was higher
 397 than that of LD at 17%-35% stage ($p < 0.001$), and lower than that of LD at 38%-49%
 398 stage ($p=0.027$). The activation of the tibialis anterior muscle was less than that of LD

399 at 17%-22% and 82%-96% stages ($p=0.041$, $p=0.001$, respectively).

400 In terms of muscle strength, the biceps femoris muscle strength of ND was lower
401 than that of LD at 48%-68% stage ($p=0.001$) and 38%-49% stage ($p < 0.001$), and the
402 rectus femoris muscle strength was lower than that of LD at 9%-30% stage and 63%-
403 100% stage ($p=0.013$, $p < 0.001$, respectively). The muscle strength of the vastus
404 medialis was higher than that of LD at 62%-83% stage ($p=0.001$), the muscle strength
405 of the vastus lateralis was higher than that of LD at 65%-86% stage ($p=0.001$), and the
406 muscle strength of the medial gastrocnemius was lower than that of LD at 83%-100%
407 stage ($p=0.001$). Soleus muscle strength was higher than LD at 34%-56% stage
408 ($p=0.023$), and the tibialis anterior muscle strength was higher than LD at 0%-8% stage
409 and 14%-31% stage ($p=0.031$, $p=0.009$, respectively).



410

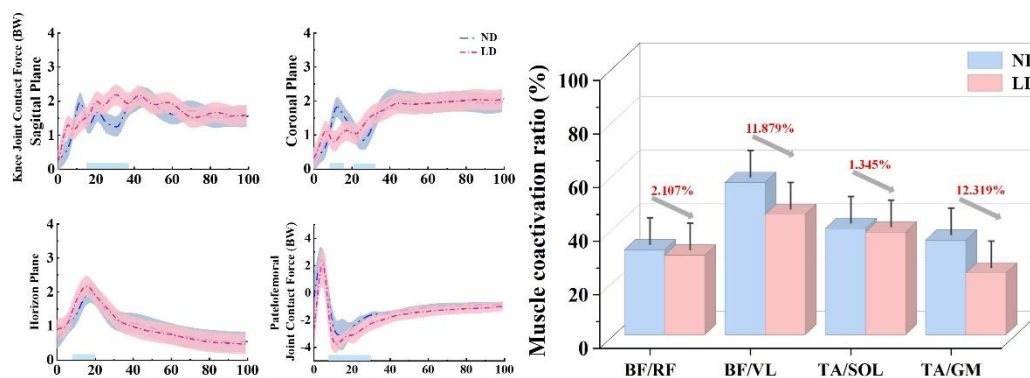
411 **Figure 5:** Illustration of the muscle activation and muscle force differences between
412 ND and LD during CMJ testing. Blue lines and "*" indicate significant differences (p
413 < 0.05).

414

415 4.3 Joint contact force and Muscle-coactivation

416 As shown in Figure 6, the differences in knee contact force, patellar joint contact
417 force, and degree of muscle coactivation around the knee between ND and LD during

418 the landing phase of the CMJ. In the sagittal plane, the knee contact force of ND was
 419 lower than that of LD in the 15%-38% stage ($p=0.034$). In the coronal plane, the knee
 420 contact force of ND was higher than that of LD in the 10%-15% stage ($p=0.028$) and
 421 lower than that of LD in the 21%-30% stage ($p=0.024$). The knee contact force in the
 422 horizontal plane was lower than that in the LD at 10%-20% stage ($p=0.028$). The
 423 contact force of ND was higher than that of LD at the stage of 8%-20% ($p < 0.001$). In
 424 terms of muscle coactivation, BF/RF, BF/VF, TA/SOL, and TA/GM of ND were
 425 2.107%, 11.879%, 11.345%, and 12.319% higher than those of LD, respectively.

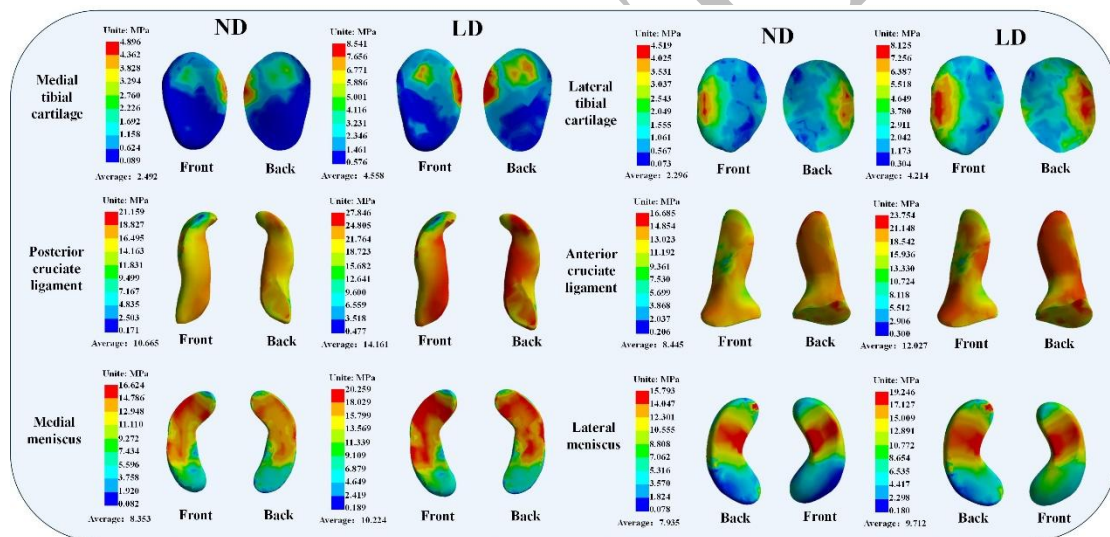


426
 427 **Figure 6:** Illustration of the knee contact force, patellar joint contact force, and muscle
 428 coactivation differences between ND and LD in the CMJ test. Blue lines and "*"
 429 indicate significant differences ($p < 0.05$).
 430

431 4.4 Finite element analysis

432 Figure 7 outlines the differences between ND and LD in the von Mises stress
 433 distributions such as ligaments and soft tissues during the landing phase of the CMJ.
 434 The average von Mises stress and the peak von Mises stress of the medial tibial cartilage
 435 in ND were 2.492MPa and 4.896MPa, respectively. The average von Mises stress and
 436 the peak von Mises stress of the medial tibial cartilage in LD were 4.558MPa and
 437 8.541MPa. The average von Mises stress and the peak von Mises stress in the lateral
 438 tibial cartilage of ND were 2.296MPa and 4.519MPa, respectively. The average von
 439 Mises stress and the peak von Mises stress in the medial tibial cartilage of LD were
 440 4.214MPa and 8.125MPa, respectively. The average von Mises stress and the peak von

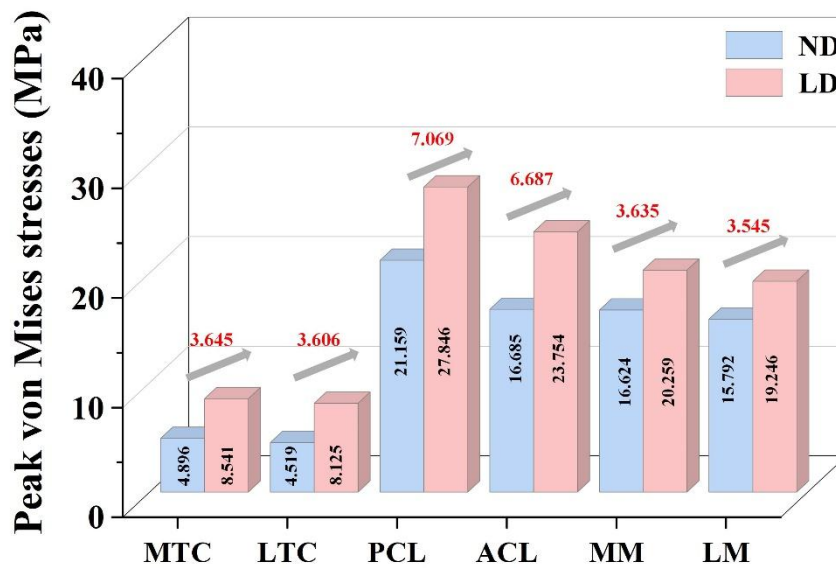
441 Mises stress of the posterior cruciate ligament in ND was 10.665MPa and 21.159MPa,
 442 respectively. The average von Mises stress and the peak von Mises stress of the
 443 posterior cruciate ligament in LD was 14.161MPa and 27.846MPa. The mean von
 444 Mises stress and the peak von Mises stress of the ACL in ND were 8.445MPa and
 445 16.685MPa, respectively. The mean von Mises stress and the peak von Mises stress of the ACL in LD
 446 were 12.027MPa and 23.754MPa. The mean von Mises stress and the peak von Mises stress of the medial meniscus in ND
 447 were 8.353MPa and 16.624MPa, respectively. The mean von Mises stress and the peak von Mises stress of the medial
 448 meniscus in LD was 10.224MPa and 20.259MPa. The mean von Mises stress and the
 449 peak von Mises stress of the lateral meniscus in ND were 7.935MPa and 15.793MPa,
 450 respectively. The mean von Mises stress and the peak von Mises stress of the lateral
 451 meniscus in LD were 9.712MPa and 19.246MPa.



453
 454 **Figure 7:** Visualization of the von Mises stress distribution of the tibial cartilage,
 455 cruciate ligaments, and menisci during the landing phase of the CMJ test for ND and
 456 LD.

457
 458 As shown in Figure 8, the differences in peak von Mises stress changes such as
 459 ligaments and soft tissues between ND and LD during the landing phase of the CMJ
 460 were observed. Compared with ND, LD increased 3.645MPa in the medial tibial
 461 cartilage, 3.606Mpa in the lateral tibial cartilage, 7.069MPa in the posterior cruciate
 462 ligament, 6.687Mpa in the anterior cruciate ligament, 3.635Mpa in the medial meniscus,

463 and 3.545Mpa in the lateral meniscus.



464
465 **Figure 8:** Visualization of von Mises peak stress changes in the tibial cartilage, cruciate
466 ligaments, and menisci during the landing phase of the CMJ test for ND and LD.

467

468 5. Discussion

469 This study investigated how varying levels of ankle dorsiflexion affect lower limb
470 biomechanics during the cushion-landing phase. We hypothesized that a reduced ankle
471 dorsiflexion ROM during landing would increase knee joint stress, thereby heightening
472 the risk of injury. Additionally, we anticipated that the knee joint would exhibit adaptive
473 changes to compensate for the limited ankle dorsiflexion. The results of this study
474 supported the initial hypothesis and revealed several key findings: (1) With a lower
475 ankle dorsiflexion ROM, the knee joint demonstrated increased adduction and external
476 rotation angles during the landing buffer phase, accompanied by higher von Mises
477 stresses in the tibial cartilage, meniscus, ACL, and PCL. (2) A reduced ankle
478 dorsiflexion ROM was associated with smaller contact forces of the patella and knee
479 joint in the horizontal plane. (3) At lower dorsiflexion ROM, muscle activation of the
480 rectus femoris, vastus medialis, and vastus lateralis was lower at certain stages, while
481 the activation of the soleus occurred later in the movement. (4) The muscle coactivation
482 around the knee joint (BF/RF, BF/VL, TA/SOL, TA/GM) was reduced when the ankle
483 joint ROM was limited.

484 During the CMJ landing, subjects typically transitioned from plantar flexion to
485 dorsiflexion of the ankle joint. The findings of this study showed that the ND group
486 displayed a greater ankle dorsiflexion angle than the LD group, whereas the LD group
487 exhibited a higher peak plantar flexion moment. These results align with previous
488 research, which has proposed that greater ankle plantarflexion may increase the ankle's
489 ROM, thus enhancing its capacity to absorb impact forces and potentially lowering the
490 risk of knee injuries [17, 36, 68]. Additionally, the LD group displayed greater knee
491 adduction and external rotation angles, as well as higher joint forces during landing.
492 The knee joint is essential for maintaining balance during dynamic movements [62],
493 with the contact force between the patella and femur being a key factor in knee stability.
494 In this study, the patellar joint contact force (PTF) was calculated using a specific
495 formula [28, 34, 60], and the results indicated that, compared to the LD group, the ND
496 group exhibited higher patellar joint contact forces at certain stages of the landing phase.
497 This phenomenon is likely attributable to the larger dorsiflexion ROM in the ND group.
498 A greater dorsiflexion angle facilitates a larger range of ankle motion, which may enable
499 the lower limbs to absorb more of the impact forces during landing [17, 29]. Previous
500 research has also shown that a limited dynamic functional ROM in the ankle joint is
501 associated with a higher risk of injury during jumping and landing activities [69]. For
502 example, healthy female athletes typically demonstrate a larger dynamic functional
503 range during landing, and modifying the initial contact angle of the ankle joint can
504 effectively lower the risk of knee injuries [42, 62].

505 In terms of muscle activation, the results of this study indicate that the LD group
506 exhibited lower muscle activation of the rectus femoris, vastus medialis, and vastus
507 lateralis at certain stages compared to the ND group, with delayed activation of the
508 soleus. Additionally, muscle coactivation around the knee joint (BF/RF, BF/VL,
509 TA/SOL, TA/GM) was lower in the LD group when ankle joint motion was limited.
510 Previous research on the effects of physical therapy for patellar tendinopathy has shown
511 that increasing ankle dorsiflexion through rehabilitation can improve knee function,
512 reduce pain, and enhance lower limb strength and stability in patients with patellar
513 tendinopathy [14]. The findings of the present study suggest that greater ankle motion

514 may contribute to enhanced knee stability and muscle control. Although no significant
515 changes were observed in knee flexion angles, adaptive coactivation of the muscles was
516 noted, suggesting that ankle motion may contribute to knee stability. These muscle
517 adaptations could enhance the peripatellar muscles' ability to withstand higher loads,
518 potentially through hypertrophy or improved efficiency in absorbing impact forces.
519 Previous studies have highlighted the importance of coactivation patterns among the
520 muscles surrounding the knee in maintaining dynamic knee stability and preventing
521 injuries [19, 30]. Muscle coactivation is crucial for converting valgus forces into joint
522 contact forces, thus protecting the knee from injury [53, 63].

523 In this study, participants' lower limbs were scanned using Helium-free MRI and
524 CT. Compared to traditional MRI, Helium-free MRI employs a cooling system with
525 zero or very low volatilization, reducing reliance on expensive and unstable liquid
526 helium, and offering a more environmentally friendly alternative [2]. Its innovative
527 magnet design supports multi-position imaging, including standing, sitting, prone, and
528 lateral lying positions, better aligning with the natural posture and biomechanical
529 characteristics of the human body. This makes it particularly suitable for examining the
530 spine, joints, and musculoskeletal system, allowing for the detection of issues that may
531 not be observable in the supine position. Multi-position MRI enhances the accuracy of
532 joint, ligament, and tendon imaging, providing a more realistic simulation of tissue
533 loading during physical activity. A finite element model of the foot and knee-integrated
534 lower extremity was developed to more accurately simulate real-life conditions and
535 calculate stress distribution in the knee joint and its surrounding structures [40]. The
536 results indicated that, in the limited dorsiflexion (LD) condition, along with an increase
537 in knee adduction and external rotation angles, there was a corresponding increase in
538 knee adduction and external rotation torques, as well as a decrease in patellar joint
539 contact forces at certain stages. Additionally, the muscle coactivation around the knee
540 joint was lower in the LD condition. The finite element analysis further revealed that
541 LD was associated with higher stress in the tibial cartilage, meniscus, ACL, and PCL
542 compared to normal dorsiflexion (ND). This suggests that as the dorsiflexion motion of
543 the ankle joint is reduced, the stress in these structures increases, resulting in greater

544 impact loading on the knee joint, which in turn heightens the risk of injury [6, 7, 41].
545 Previous research has indicated that a reduced plantar flexion angle of the ankle during
546 landing may elevate the risk of ACL injury [36, 67]. The present findings demonstrated
547 that ACL stress was primarily concentrated in the attachment areas of the femur and
548 tibia, as well as in the medial and lateral regions. Notably, ACL tears are frequently
549 observed in the femoral attachment area [22, 46]. In conclusion, the findings of this
550 study indicate that restricted ankle dorsiflexion during landing results in heightened
551 stress on the meniscus and femoral cartilage, which in turn increases the impact load
552 on the knee joint and elevates the risk of knee injuries. These findings highlight the
553 importance of modifying ankle joint motion, particularly increasing ankle dorsiflexion,
554 to effectively reduce knee joint pressure and lower the likelihood of sports-related
555 injuries.

556 The limitations of the present study must be acknowledged. First, the initial data
557 collection through CT and MRI involved a cohort of male participants in good health.
558 Due to inherent individual differences, the results of this study may not be universally
559 applicable and could vary across different populations. Additionally, the simulation of
560 the tibial ACL as a linear elastic material may have influenced the accuracy of the
561 results for these ligaments. This simplification, however, is commonly used in prior
562 research to improve computational efficiency. Furthermore, the study was conducted
563 under controlled laboratory conditions, which may not fully reflect the conditions
564 encountered in actual competitive settings. Future studies should aim to conduct
565 experiments under conditions that more closely simulate real-world competitive
566 environments to improve the external validity of the findings. Meanwhile this study
567 included 32 male basketball players, the sample size—although likely sufficient for
568 certain analyses—may still benefit from a larger and more diverse cohort, including
569 different genders and athletes of varying competitive levels, to enhance the statistical
570 power and generalizability of the results.

571 Future research can further optimize computational modeling and simulation to
572 enhance the precision of personalized injury risk prediction and the realism of
573 biomechanical simulations. First, a more refined foot-knee-hip integrated model can be

574 developed to extend the current knee-focused analysis, enabling a comprehensive
575 investigation of lower limb kinetic chains and the interplay between the hip, knee, and
576 ankle injury mechanisms [67]. Second, machine learning and deep learning algorithms
577 can be incorporated to optimize musculoskeletal modeling and FEA parameters,
578 leveraging individualized biomechanical data to improve injury risk prediction and
579 develop personalized intervention strategies [70]. Finally, wearable sensor technology
580 (e.g., inertial measurement units and pressure insoles) can be employed to capture real-
581 world biomechanical data during competitive play, facilitating validation of simulation
582 models and enhancing their applicability and predictive accuracy in dynamic sports
583 environments.

584

585 **6. Conclusions**

586 This study explored how different levels of ankle dorsiflexion affect knee joint
587 impact load during landing, utilizing a personalized musculoskeletal model and a finite
588 element model that integrates the foot and knee. The results indicate that greater ankle
589 dorsiflexion during landing may effectively reduce internal tissue stress in the knee joint
590 and enhance muscle coactivation around the knee, as well as increase the patellar joint
591 contact force. These findings provide valuable theoretical support for strategies to
592 reduce the risk of knee injuries during landing. Moreover, they offer reliable technical
593 methods and theoretical references for the study of injury mechanisms in other athletic
594 activities, such as running and lateral jumping.

595

596 **Data availability**

597 All data relevant to the current study are included in the article, further inquiries
598 can be directed at the corresponding author.

599

600 **Funding**

601 This study was sponsored by the Ningbo key R&D Program (2022Z196), Research
602 Academy of Medicine Combining Sports, Ningbo (No.2023001), the Project of
603 NINGBO Leading Medical &Health Discipline (No.2022-F15, No.2022-F22), Ningbo

604 Natural Science Foundation (2022J065, 20221JCGY010607), Public Welfare Science
605 & Technology Project of Ningbo, China (2021S134), and Zhejiang Rehabilitation
606 Medical Association Scientific Research Special Fund (ZKKY2023001).

607

608 **References**

609 [1] Backman LJ., Danielson P., Low range of ankle dorsiflexion predisposes for
610 patellar tendinopathy in junior elite basketball players: a 1-year prospective study,
611 The American journal of sports medicine, 2011, 39(12), 2626-33, DOI:
612 10.1177/0363546511420552.

613 [2] Bagdinova A., Rybakov A., Demikhov E., Demikhov T., Lysenko V., Tarasov V.,
614 Shumm B., Dmitriev D., Simulation of a Gradient System for a Helium-Free
615 Magnetic Resonance Imager, Instruments and Experimental Techniques, 2022,
616 65(1), 113-22, DOI: 10.1134/S0020441222010018.

617 [3] Baldwin MA., Clary CW., Fitzpatrick CK., Deacy JS., Maletsky LP., Rullkoetter
618 PJ., Dynamic finite element knee simulation for evaluation of knee replacement
619 mechanics, Journal of biomechanics, 2012, 45(3), 474-83, DOI:
620 10.1016/j.jbiomech.2011.11.052.

621 [4] Bendjaballah MZ., Shirazi-Adl A., Zukor D., Biomechanics of the human knee
622 joint in compression: reconstruction, mesh generation and finite element analysis,
623 The knee, 1995, 2(2), 69-79, DOI: 10.1016/0968-0160(95)00018-K.

624 [5] Benos L., Stanev D., Spyrou L., Moustakas K., Tsaopoulos DE., A review on finite
625 element modeling and simulation of the anterior cruciate ligament reconstruction,
626 Frontiers in Bioengineering and Biotechnology, 2020, 8, 967, DOI:
627 10.3389/fbioe.2020.00967.

628 [6] Buckwalter JA., Sports, joint injury, and posttraumatic osteoarthritis, Journal of
629 Orthopaedic & Sports Physical Therapy, 2003, 33(10), 578-88, DOI:
630 10.2519/jospt.2003.33.10.578.

631 [7] Buckwalter JA., Anderson DD., Brown TD., Tochigi Y., Martin JA., The roles of
632 mechanical stresses in the pathogenesis of osteoarthritis: implications for treatment
633 of joint injuries, Cartilage, 2013, 4(4), 286-94, DOI: 10.1177/1947603513495889.

- 634 [8] Chandran AS., Trivedi R., Modi B., Patel R., Estimation of stress and strain of knee
635 joint using finite element analysis, *Journal of Physics: Conference Series*; 2021,
636 012217, DOI: 10.1088/1742-6596/2070/1/012217.
- 637 [9] Chen W-M., Lee T., Lee PV-S., Lee JW., Lee S-J., Effects of internal stress
638 concentrations in plantar soft-tissue—a preliminary three-dimensional finite
639 element analysis, *Medical engineering & physics*, 2010, 32(4), 324-31, DOI:
640 10.1016/j.medengphy.2010.01.001.
- 641 [10] Chen W-M., Park J., Park S-B., Shim VP-W., Lee T., Role of gastrocnemius–soleus
642 muscle in forefoot force transmission at heel rise—A 3D finite element analysis,
643 *Journal of biomechanics*, 2012, 45(10), 1783-9, DOI:
644 10.1016/j.jbiomech.2012.04.024.
- 645 [11] Cheung JT-M., Zhang M., A 3-dimensional finite element model of the human foot
646 and ankle for insole design, *Archives of physical medicine and rehabilitation*, 2005,
647 86(2), 353-8, DOI: 10.1016/j.apmr.2004.03.031.
- 648 [12] Cheung JT-M., Zhang M., Leung AK-L., Fan Y-B., Three-dimensional finite
649 element analysis of the foot during standing—a material sensitivity study, *Journal*
650 *of biomechanics*, 2005, 38(5), 1045-54, DOI: 10.1016/j.jbiomech.2004.05.035.
- 651 [13] Cheung JT-M., Yu J., Wong DW-C., Zhang M., Current methods in computer-aided
652 engineering for footwear design, *Footwear science*, 2009, 1(1), 31-46, DOI:
653 10.1080/19424280903002323.
- 654 [14] Coelho BAL., Das Neves Rodrigues HL., Almeida GPL., João SMA., Immediate
655 effect of ankle mobilization on range of motion, dynamic knee valgus, and knee
656 pain in women with patellofemoral pain and ankle dorsiflexion restriction: a
657 randomized controlled trial with 48-hour follow-up, *Journal of Sport Rehabilitation*,
658 2021, 30(5), 697-706, DOI: 10.1123/jsr.2020-0183.
- 659 [15] De Asla RJ., Kozánek M., Wan L., Rubash HE., Li G., Function of anterior
660 talofibular and calcaneofibular ligaments during in-vivo motion of the ankle joint
661 complex, *Journal of Orthopaedic Surgery and Research*, 2009, 4, 1-6, DOI:
662 10.1186/1749-799X-4-7.
- 663 [16] Dufek JS., Bates BT., Biomechanical factors associated with injury during landing

- 664 in jump sports, *Sports medicine*, 1991, 12, 326-37, DOI: 10.2165/00007256-
665 199112050-00005.
- 666 [17]Fong C-M., Blackburn JT., Norcross MF., McGrath M., Padua DA., Ankle-
667 dorsiflexion range of motion and landing biomechanics, *Journal of athletic training*,
668 2011, 46(1), 5-10, DOI: 10.4085/1062-6050-46.1.5.
- 669 [18]Gabriel MT., Wong EK., Woo SLY., Yagi M., Debski RE., Distribution of in situ
670 forces in the anterior cruciate ligament in response to rotatory loads, *Journal of*
671 *orthopaedic research*, 2004, 22(1), 85-9, DOI: 10.1016/S0736-0266(03)00133-5.
- 672 [19]Gao X., Xu D., Baker JS., Ee-Chon T., Liang M., Gu Y., Exploring biomechanical
673 variations in ankle joint injuries among Latin dancers with different stance patterns:
674 utilizing OpenSim musculoskeletal models, *Frontiers in Bioengineering and*
675 *Biotechnology*, 2024, 12, 1359337, DOI: 10.3389/fbioe.2024.1359337.
- 676 [20]Gardiner JC., Weiss JA., Rosenberg TD., Strain in the human medial collateral
677 ligament during valgus loading of the knee, *Clinical Orthopaedics and Related*
678 *Research*, 2001, 391, 266-74, DOI: 10.1097/00003086-200110000-00031.
- 679 [21]Gillen ZM., Jahn LE., Shoemaker ME., McKay BD., Mendez AI., Bohannon NA.,
680 Cramer JT., Effects of eccentric preloading on concentric vertical jump
681 performance in youth athletes, *Journal of applied biomechanics*, 2019, 35(5), 327-
682 35, DOI: 10.1123/jab.2018-0340.
- 683 [22]Giron F., Cuomo P., Aglietti P., Bull AM., Amis AA., Femoral attachment of the
684 anterior cruciate ligament, *Knee Surgery, Sports Traumatology, Arthroscopy*, 2006,
685 14, 250-6, DOI: 10.1007/s00167-005-0685-y.
- 686 [23]Godest A., Beaugonin M., Haug E., Taylor M., Gregson P., Simulation of a knee
687 joint replacement during a gait cycle using explicit finite element analysis, *Journal*
688 *of biomechanics*, 2002, 35(2), 267-75, DOI: 10.1016/S0021-9290(01)00179-8.
- 689 [24]Gu Y., Ren X., Li J., Lake M., Zhang Q., Zeng Y., Computer simulation of stress
690 distribution in the metatarsals at different inversion landing angles using the finite
691 element method, *International orthopaedics*, 2010, 34, 669-76, DOI:
692 10.1007/s00264-009-0856-4.
- 693 [25]Hall EA., Docherty CL., Validity of clinical outcome measures to evaluate ankle

- 694 range of motion during the weight-bearing lunge test, *Journal of science and*
695 *medicine in sport*, 2017, 20(7), 618-21, DOI: 10.1016/j.jsams.2016.11.001.
- 696 [26]Halloran JP., Petrella AJ., Rullkoetter PJ., Explicit finite element modeling of total
697 knee replacement mechanics, *Journal of biomechanics*, 2005, 38(2), 323-31, DOI:
698 10.1016/j.jbiomech.2004.02.046.
- 699 [27]Haut Donahue TL., Hull M., Rashid MM., Jacobs CR., A finite element model of
700 the human knee joint for the study of tibio-femoral contact, *J Biomech Eng*, 2002,
701 124(3), 273-80, DOI: 10.1115/1.1470171.
- 702 [28]Ho K-Y., Blanchette MG., Powers CM., The influence of heel height on
703 patellofemoral joint kinetics during walking, *Gait & posture*, 2012, 36(2), 271-5,
704 DOI: 10.1016/j.gaitpost.2012.03.008.
- 705 [29]Hoch MC., Farwell KE., Gaven SL., Weinhandl JT., Weight-bearing dorsiflexion
706 range of motion and landing biomechanics in individuals with chronic ankle
707 instability, *Journal of athletic training*, 2015, 50(8), 833-9, DOI: 10.4085/1062-
708 6050-50.5.07.
- 709 [30]Hubley-Kozey C., Deluzio K., Dunbar M., Muscle co-activation patterns during
710 walking in those with severe knee osteoarthritis, *Clinical biomechanics*, 2008,
711 23(1), 71-80, DOI: 10.1016/j.clinbiomech.2007.08.019.
- 712 [31]Kang Z., Jiang X., The effect of running experience on muscle forces and knee
713 joint reaction forces during running, *International Journal of Biomedical*
714 *Engineering and Technology*, 2024, 45(3), 183-197, DOI:
715 10.1504/IJBET.2024.138969.
- 716 [32]Knörlein BJ., Baier DB., Gatesy SM., Laurence-Chasen J., Brainerd EL.,
717 Validation of XMA Lab software for marker-based XROMM, *Journal of*
718 *Experimental Biology*, 2016, 219(23), 3701-11, DOI: 10.1242/jeb.145383.
- 719 [33]Koyama T., Rikukawa A., Nagano Y., Sasaki S., Ichikawa H., Hirose N.,
720 Acceleration profile of high-intensity movements in basketball games, *The Journal*
721 *of Strength & Conditioning Research*, 2022, 36(6), 1715-9, DOI:
722 10.1519/JSC.0000000000003699.
- 723 [34]Kubo K., Miyazaki D., Tanaka S., Shimoju S., Tsunoda N., Relationship between

- 724 Achilles tendon properties and foot strike patterns in long-distance runners, *Journal*
725 *of Sports Sciences*, 2015, 33(7), 665-9, DOI: 10.1080/02640414.2014.962576.
- 726 [35]Lee J., Song Y., Shin CS., Effect of the sagittal ankle angle at initial contact on
727 energy dissipation in the lower extremity joints during a single-leg landing, *Gait &*
728 *posture*, 2018, 62, 99-104, DOI: 10.1016/j.gaitpost.2018.03.019.
- 729 [36]Leppänen M., Pasanen K., Krosshaug T., Kannus P., Vasankari T., Kujala UM.,
730 Bahr R., Perttunen J., Parkkari J., Sagittal plane hip, knee, and ankle biomechanics
731 and the risk of anterior cruciate ligament injury: a prospective study, *Orthopaedic*
732 *journal of sports medicine*, 2017, 5(12), 2325967117745487, DOI:
733 10.1177/2325967117745487.
- 734 [37]LeRoux MA., Setton LA., Experimental and biphasic FEM determinations of the
735 material properties and hydraulic permeability of the meniscus in tension, *J*
736 *Biomech Eng*, 2002, 124(3), 315-21, DOI: 10.1115/1.1468868.
- 737 [38]Li G., Lopez O., Rubash H., Variability of a three-dimensional finite element model
738 constructed using magnetic resonance images of a knee for joint contact stress
739 analysis, *J Biomech Eng*, 2001, 123(4), 341-6, DOI: 10.1115/1.1385841.
- 740 [39]Li G., Van de Velde SK., Bingham JT., Validation of a non-invasive fluoroscopic
741 imaging technique for the measurement of dynamic knee joint motion, *Journal of*
742 *biomechanics*, 2008, 41(7), 1616-22, DOI: 10.1115/1.1385841.
- 743 [40]Liu X., Zhang M., Redistribution of knee stress using laterally wedged insole
744 intervention: Finite element analysis of knee–ankle–foot complex, *Clinical*
745 *Biomechanics*, 2013, 28(1), 61-7, DOI: 10.1016/j.clinbiomech.2012.10.004.
- 746 [41]Logerstedt DS., Ebert JR., MacLeod TD., Heiderscheid BC., Gabbett TJ.,
747 Eckenrode BJ., Effects of and Response to Mechanical Loading on the Knee,
748 *Sports Medicine*, 2022, 52(2), 201-35, DOI: 10.1007/s40279-021-01579-7.
- 749 [42]Malloy P., Morgan A., Meinerz C., Geiser C., Kipp K., The association of
750 dorsiflexion flexibility on knee kinematics and kinetics during a drop vertical jump
751 in healthy female athletes, *Knee Surgery, Sports Traumatology, Arthroscopy*, 2015,
752 23, 3550-5, DOI: 10.1007/s00167-014-3222-z.
- 753 [43]Markovic G., Dizdar D., Jukic I., Cardinale M., Reliability and factorial validity of

754 squat and countermovement jump tests, *The Journal of Strength & Conditioning*
755 *Research*, 2004, 18(3), 551-5, DOI: 10.1519/1533-
756 4287(2004)18<551:RAFVOS>2.0.CO;2.

757 [44] Márquez G., Aguado X., Alegre LM., Fernández-del-Olmo M., Neuromechanical
758 adaptation induced by jumping on an elastic surface, *Journal of electromyography*
759 *and kinesiology*, 2013, 23(1), 62-9, DOI: 10.1016/j.jelekin.2012.06.012.

760 [45] Marshall J., Bishop C., Turner A., Haff GG., Optimal training sequences to develop
761 lower body force, velocity, power, and jump height: A systematic review with meta-
762 analysis, *Sports Medicine*, 2021, 51, 1245-71, DOI: 10.1007/s40279-021-01430-z.

763 [46] Muneta T., Koga H., Nakamura T., Horie M., Watanabe T., Sekiya I., Behind-
764 remnant arthroscopic observation and scoring of femoral attachment of injured
765 anterior cruciate ligament, *Knee Surgery, Sports Traumatology, Arthroscopy*, 2016,
766 24, 2906-14, DOI: 10.1007/s00167-015-3574-z.

767 [47] Norcross MF., Almog R., Huang Y-L., Chang E., Hannigan KS., Johnson ST.,
768 Greater explosive quadriceps strength is associated with greater knee flexion at
769 initial contact during landing in females, *Sports biomechanics*, 2024, 23(8), 1028-
770 42, DOI: 10.1080/14763141.2021.1908413.

771 [48] Nuzzo JL., McBride JM., Cormie P., McCaulley GO., Relationship between
772 countermovement jump performance and multijoint isometric and dynamic tests of
773 strength, *The Journal of Strength & Conditioning Research*, 2008, 22(3), 699-707,
774 DOI: 10.1080/14763141.2021.1908413.

775 [49] Ota S., Ueda M., Aimoto K., Suzuki Y., Sigward S., Acute influence of restricted
776 ankle dorsiflexion angle on knee joint mechanics during gait, *The Knee*, 2014,
777 21(3), 669-75, DOI: 10.1016/j.knee.2014.01.006.

778 [50] Pailler-Mattei C., Bec S., Zahouani H., In vivo measurements of the elastic
779 mechanical properties of human skin by indentation tests, *Medical engineering &*
780 *physics*, 2008, 30(5), 599-606, DOI: 10.1016/j.medengphy.2007.06.011.

781 [51] Pena E., Calvo B., Martinez M., Doblare M., A three-dimensional finite element
782 analysis of the combined behavior of ligaments and menisci in the healthy human
783 knee joint, *Journal of biomechanics*, 2006, 39(9), 1686-701, DOI:

784 10.1016/j.jbiomech.2005.04.030.

785 [52]Petrigna L., Karsten B., Marcolin G., Paoli A., D'Antona G., Palma A., Bianco A.,
786 A review of countermovement and squat jump testing methods in the context of
787 public health examination in adolescence: reliability and feasibility of current
788 testing procedures, *Frontiers in physiology*, 2019, 10, 1384, DOI:
789 10.3389/fphys.2019.01384.

790 [53]Podraza JT., White SC., Effect of knee flexion angle on ground reaction forces,
791 knee moments and muscle co-contraction during an impact-like deceleration
792 landing: implications for the non-contact mechanism of ACL injury, *The Knee*,
793 2010, 17(4), 291-5, DOI: 10.1016/j.knee.2010.02.013.

794 [54]Powden CJ., Hoch JM., Hoch MC., Reliability and minimal detectable change of
795 the weight-bearing lunge test: a systematic review, *Manual therapy*, 2015, 20(4),
796 524-32, DOI: 10.1016/j.math.2015.01.004.

797 [55]Sanna G., O'Connor KM., Fatigue-related changes in stance leg mechanics during
798 sidestep cutting maneuvers, *Clinical biomechanics*, 2008, 23(7), 946-54, DOI:
799 10.1016/j.clinbiomech.2008.03.065.

800 [56]Seth A., Hicks JL., Uchida TK., Habib A., Dembia CL., Dunne JJ., Ong CF.,
801 DeMers MS., Rajagopal A., Millard M., OpenSim: Simulating musculoskeletal
802 dynamics and neuromuscular control to study human and animal movement, *PLoS*
803 *computational biology*, 2018, 14(7), e1006223, DOI:
804 10.1371/journal.pcbi.1006223.

805 [57]Siegler S., Block J., Schneck CD., The mechanical characteristics of the collateral
806 ligaments of the human ankle joint, *Foot & ankle*, 1988, 8(5), 234-42, DOI:
807 10.1177/107110078800800502.

808 [58]Song Y., Debski RE., Musahl V., Thomas M., Woo SL-Y., A three-dimensional
809 finite element model of the human anterior cruciate ligament: a computational
810 analysis with experimental validation, *Journal of biomechanics*, 2004, 37(3), 383-
811 90, DOI: 10.1016/S0021-9290(03)00261-6.

812 [59]Suggs J., Wang C., Li G., The effect of graft stiffness on knee joint biomechanics
813 after ACL reconstruction—a 3D computational simulation, *Clinical biomechanics*,

- 814 2003, 18(1), 35-43, DOI: 10.1016/S0268-0033(02)00137-7.
- 815 [60] Van Eijden T., De Boer W., Weijs W., The orientation of the distal part of the
816 quadriceps femoris muscle as a function of the knee flexion-extension angle,
817 Journal of biomechanics, 1985, 18(10), 803-9, DOI: 10.1016/0021-
818 9290(85)90055-7.
- 819 [61] Wang H-K., Chen C-H., Shiang T-Y., Jan M-H., Lin K-H., Risk-factor analysis of
820 high school basketball–player ankle injuries: A prospective controlled cohort study
821 evaluating postural sway, ankle strength, and flexibility, Archives of physical
822 medicine and rehabilitation, 2006, 87(6), 821-5, DOI: 10.1016/j.apmr.2006.02.024.
- 823 [62] Wikstrom EA., Tillman MD., Chmielewski TL., Borsa PA., Measurement and
824 evaluation of dynamic joint stability of the knee and ankle after injury, Sports
825 medicine, 2006, 36, 393-410, DOI: 10.2165/00007256-200636050-00003.
- 826 [63] Wilczyński B., Zorena K., Ślęzak D., Dynamic knee valgus in single-leg movement
827 tasks. Potentially modifiable factors and exercise training options. A literature
828 review, International journal of environmental research and public health, 2020,
829 17(21), 8208, DOI: 10.3390/ijerph17218208.
- 830 [64] Xu D., Lu J., Baker JS., Fekete G., Gu Y., Temporal kinematic and kinetics
831 differences throughout different landing ways following volleyball spike shots,
832 Proceedings of the Institution of Mechanical Engineers, Journal of Sports
833 Engineering and Technology, 2022, 236(3), 200-8, DOI:
834 10.1177/17543371211009485.
- 835 [65] Xu D., Quan W., Zhou H., Sun D., Baker JS., Gu Y., Explaining the differences of
836 gait patterns between high and low-mileage runners with machine learning,
837 Scientific reports, 2022, 12(1), 2981, DOI: 10.1038/s41598-022-07054-1.
- 838 [66] Xu D., Zhou H., Quan W., Gusztav F., Baker JS., Gu Y., Adaptive neuro-fuzzy
839 inference system model driven by the non-negative matrix factorization-extracted
840 muscle synergy patterns to estimate lower limb joint movements, Computer
841 Methods and Programs in Biomedicine, 2023, 242, 107848, DOI:
842 10.1016/j.cmpb.2023.107848.
- 843 [67] Xu D., Zhou H., Quan W., Gusztav F., Wang M., Baker JS., Gu Y., Accurately and

844 effectively predict the ACL force: Utilizing biomechanical landing pattern before
845 and after-fatigue, *Computer Methods and Programs in Biomedicine*, 2023, 241,
846 107761, DOI: 10.1016/j.cmpb.2023.107761.

847 [68] Xu D., Zhou H., Wang M., Ma X., Gusztav F., Chon T-E., Fernandez J., Baker JS.,
848 Gu Y., Contribution of ankle motion pattern during landing to reduce the knee-
849 related injury risk, *Computers in Biology and Medicine*, 2024, 180, 108965, DOI:
850 10.1016/j.compbimed.2024.108965.

851 [69] Xu D., Zhou H., Quan W., Ma X., Chon T-E., Fernandez J., Gusztav F., Kovács A.,
852 Baker JS., Gu Y., New insights optimize landing strategies to reduce lower limb
853 injury risk, *Cyborg and Bionic Systems*, 2024, 5, 0126, DOI:
854 10.34133/cbsystems.0126.

855 [70] Xu D., Zhou H., Quan W., Jiang X., Liang M., Li S., Ugbolue UC., Baker JS.,
856 Gusztav F., Ma X., A new method proposed for realizing human gait pattern
857 recognition: Inspirations for the application of sports and clinical gait analysis, *Gait
858 & Posture*, 2024, 107, 293-305, DOI: 10.1016/j.gaitpost.2023.10.019.

859 [71] Yan M., Liang T., Zhao H., Bi Y., Wang T., Yu T., Zhang Y., Model Properties and
860 Clinical Application in the Finite Element Analysis of Knee Joint: A Review,
861 *Orthopaedic Surgery*, 2024, 16(2), 289-302, DOI: 10.1111/os.13980.

862 [72] Yeow CH., Lee PVS., Goh JCH., An investigation of lower extremity energy
863 dissipation strategies during single-leg and double-leg landing based on sagittal
864 and frontal plane biomechanics, *Human movement science*, 2011, 30(3), 624-35,
865 DOI: 10.1016/j.humov.2010.11.010.

866 [73] Zhang Q., Zhang Y., Chon TE., Baker JS., Gu Y., Analysis of stress and stabilization
867 in adolescent with osteoporotic idiopathic scoliosis: Finite element method,
868 *Computer Methods in Biomechanics and Biomedical Engineering*, 2023, 26(1), 12-
869 24, DOI: 10.1080/10255842.2022.2044803.

870 [74] Zhang S-N., Bates BT., Dufek JS., Contributions of lower extremity joints to
871 energy dissipation during landings, *Medicine and science in sports and exercise*,
872 2000, 32(4), 812-9, DOI: 10.1097/00005768-200004000-00014.

873 [75] Zhang Z., Xu D., Gao X., Liang M., Baker JS., Gu Y., The Effect of Different

874 Degrees of Ankle Dorsiflexion Restriction on the Biomechanics of the Lower
875 Extremity in Stop-Jumping, *Applied Bionics and Biomechanics*, 2024, 2024(1),
876 9079982, DOI: 10.1155/2024/9079982.

877 [76]Zhou H., Ugbolue UC., Biomechanical analysis of lower limbs based on unstable
878 condition sports footwear: a systematic review, *Physical Activity and Health*, 2024,
879 8(1), DOI: 10.5334/paah.332.

880 [77]Zhou H., Xu D., Quan W., Ugbolue UC., Gu Y., Effects of different contact angles
881 during forefoot running on the stresses of the foot bones: a finite element simulation
882 study, *Frontiers in Bioengineering and Biotechnology*, 2024, 12, 1337540, DOI:
883 10.3389/fbioe.2024.1337540.

884 [78]Zhou H., Xu D., Chen C., Ugbolue UC., Baker JS., Gu Y., Analysis of different
885 stop-jumping strategies on the biomechanical changes in the lower limbs, *Applied*
886 *Sciences*, 2021, 11(10), 4633, DOI: 10.3390/app11104633.

887 [79]Zhou H., Xu D., Quan W., Ugbolue UC., Zhou Z., Gu Y., Can the entire function
888 of the foot Be concentrated in the forefoot area during the running stance phase? A
889 finite element study of different shoe soles, *Journal of Human Kinetics*, 2023, 92,
890 5, DOI: 10.5114/jhk/174311.

891 [80]Zhou Z., Zhou H., Jie T., Xu D., Teo E-C., Wang M., Gu Y., Analysis of stress
892 response distribution in patients with lateral ankle ligament injuries: a study of
893 neural control strategies utilizing predictive computing models, *Frontiers in*
894 *Physiology*, 2024, 15, 1438194, DOI: 10.3389/fphys.2024.1438194.